Low-Noise Thrust Generation by Laser-Ablative Micropropulsion

IEPC-2015-143／ISTS-2015-b-143

Presented at Joint Conference of 30th International Symposium on Space Technology and Science, 34th International Electric Propulsion Conference and 6th Nano-satellite Symposium
Hyogo-Kobe, Japan
July 4–10, 2015

Stefan Scharring*, Stephanie Karg†, Raoul-Amadeus Lorbeer‡, Nancy Dahms§,
and Hans-Albert Eckel¶
German Aerospace Center (DLR), Stuttgart, 70569, Germany

Abstract: Aiming for the generation of high-precision thrust in the μN range, laser-induced ablation of propellant material is employed in order to reduce thrust noise by avoiding moving parts inside the thruster. Focused high-intensity laser pulses are used for thrust generation by the recoil of the jet of the ablated material. Whereas a single laser pulse yields an extremely low impulse bit down to 1 nNs in a 40 μm focal spot on aluminum, a broad thrust range can be accessed by the variation of the laser pulse repetition rate up to several hundreds of kilohertz. Thrust measurements with a highly sensitive torsional balance, calibrated by photon pressure, yield coupling coefficients up to 15 μN per Watt average laser power and beyond. The concept of 3D electro-optical beam-steering is discussed which is essential to ablate every part of the propellant. A detailed study for the determination of the optimum laser parameters is carried out.

Nomenclature

A	= mean atomic mass
A_s	= laser spot area
$a_{1,2}$	= datafit parameters
$b_{1,2}$	= datafit parameters
$c_{1,2}$	= datafit parameters
c_e	= specific heat of the electron subsystem
c_i	= specific heat of the ion lattice
c_m	= impulse coupling coefficient
$c_{t/p}$	= thrust-to-power ratio
d_{HAZ}	= extension of the heat-affected zone
d_s	= laser spot diameter
E_L	= laser pulse energy
F	= thrust

*Senior scientist, Institute of Technical Physics, Department of Studies and Concepts, stefan.scharring@dlr.de.
†Scientist, Institute of Technical Physics, Department of Studies and Concepts, stephanie.karg@dlr.de.
‡Scientist, Institute of Technical Physics, Department of Studies and Concepts, raoul.lorbeer@dlr.de.
§Diploma student, parted from: Institute of Technical Physics, Department of Studies and Concepts.
¶Senior scientist, Head of department, Institute of Technical Physics, Department of Studies and Concepts, hans-albert.eckel@dlr.de.

f_{rep} = laser pulse repetition rate
g = Earth's gravitational acceleration
I_{sp} = specific impulse
M = propellant consumption
m = ablated mass
P_{el} = electrical power
P_L = optical power
Δp = impulse bit
R = target reflectivity at room temperature
r = radial coordinate
$\vec{r}$ = position vector
t = time
S = laser pulse energy density
T = transmissivity to the ablation region
T_e = electron temperature
T_i = ion temperature
v_{jet} = jet velocity
x = spatial x coordinate
y = spatial y coordinate
Z = degree of ionization
z = spatial z coordinate
α = optical absorption coefficient
γ_{ei} = electron-phonon coupling coefficient
η_{eo} = electro-optical energy conversion efficiency
ϑ = laser beam incidence angle
κ_e = electron heat conductivity
λ = laser wavelength
μ_a = mass areal density
ξ = normalized fluence
ξ_{opt} = normalized fluence for optimum impulse coupling
ϱ = density of the ablated material
τ_e = cooling time of the electron subsystem
τ_i = electron-phonon coupling time
τ_L = laser pulse length
Φ_{opt} = laser fluence for optimum impulse coupling
Φ_T = laser fluence at the target surface
Φ_0 = threshold fluence for laser ablation
Ψ = mass-weighted ionization factor

I. Introduction

MICROTHRUSTERS cover a great field of in-space applications where high precision in attitude and orbit control is required. Therefore, thruster specifications exhibit a broad range of mission-dependent parameters which are crucial for the selection of the appropriate propulsion technology. In the case of drag free ultra-high precision missions as, e.g., eLISA and the follow-ons of GOCE and GRACE, the demands for long-term stability, thrust vector accuracy, and high thrust resolution in conjunction with low thrust noise constitute a great challenge for cutting-edge research and development. Common requirements in thrust accuracy are in the sub-μN range. The formerly planed LISA mission for example demanded for thrust noise below 0.1 $\mu\mathrm{N}/\sqrt{\mathrm{Hz}}$ at specific impulses surpassing 500 s. Furthermore, total thrust may range up to 100 μN.[1] Similar requirements can be expected for the replacing mission eLISA.

In our conceptual study, laser-induced ablation of metals like aluminum, copper and gold is investigated under various aspects: A detailed study for the determination of the optimum working point with respect to fluence on the target surface (approx. 1 to 10 J/cm^2) is carried out. Experimental data are put into relation with findings from hydrodynamic (HD) simulations that cover a great range of parameter variations with respect to laser pulse length, laser wavelength, beam incidence angle and polarization as well.

II. Thruster Concept

In Beamed-Energy Propulsion, laser light as well as microwave radiation, either from a remote source or on-board the spacecraft, is employed for heating and acceleration of propellant material, in some cases after ablation from a solid or liquid target.[2] Basically, this propulsion concept can be referred to as electro-thermal propulsion, like, e.g., resistojet or arcjet thrusters, in contrast to electromagnetic or electrostatic thrusters.[3] Whereas this classification of electric propulsion technologies follows the common aerospace conventions, the special features of laser propulsion can be highlighted if a revised classification in terms of electrodynamics is undertaken, as shown in Fig. 1 a).

The category of near field electrodynamics can be separated into magnetic (M), high voltage (HV) and radio frequency (RF) methods. Far field dynamics have so far been explored extensively in the light frequency (LF) regime.[2] Prominent continuous thruster technologies are ion (ION) thrusters,[3] Hall-Effect ion (HALL ION) thrusters,[3] high efficient multistage plasma (HEMP) thrusters,[4] magnetoplasmadynamic[3] radio frequency thrusters as, e.g., VASIMR®[5] and radio frequency ion (RF ION) thrusters.[6] Other at least partially pulsed thruster technologies are pulsed plasma (PP) thrusters,[3,7] ion spray (ION SPRAY) or colloid thrusters,[3] laser-ablative pulsed plasma (LA PP) thrusters[7] and as a member of laser propulsion (LP),[2] laser-ablative (LA) thrusters.[2,8]

By using light frequencies (LF) of the electromagnetic spectrum it is possible to benefit from far-field technologies as, e.g., mirrors and lenses. This let alone would not be sufficient for a functioning microthruster due to the lack of an adequate light source. Nevertheless, modern laser-optical technologies allow for the preparation of highly specialized electromagnetic fields. Wavelength, temporal and spacial behavior as well as the peak power can be controlled with exquisite accuracy. This competence allows to achieve peak surface power densities surpassing 250 TW/m^2 which corresponds to approximately 300 V/μm electrical field strength. Finally, an optical approach bears the potential of omitting any moving components which present a significant source of thrust noise in many thruster concepts.

Using laser-induced ablation of propellant material, we intend to reduce motion inside the thruster to the movement of electrons, photons and propellant, thus minimizing thrust noise. The basic thruster principle is sketched in Fig. 1 b): A pulsed solid-state laser source is used to ablate and accelerate little amounts from the surface of a metallic propellant target inducing very small impulse bits. For this purpose, the laser beam is focused by an object lens and deflected towards the target surface by a mirror. Since the pulse repetition rate can be varied over several orders of magnitude, e.g., from 100 Hz to 100 kHz, a broad range of thrust levels can be accessed by selection of the appropriate frequency of ablation events corresponding to the impulse bit. This requires an careful selection of laser parameters that match the propellant material.

Electro-optical components enable deflection (EO2) and focusing (EO3) the laser beam without any mechanical motion but only by applying the suitable voltage to the corresponding device. Hence, the propellant surface cannot only be scanned in two dimensions. The variable focus length of the system of EO3 and objective allows for ablation of the target surface layer by layer as with strip mining. In order to ensure reproducible amount and direction of the imparted thrust, the scanning pattern of the laser ablation

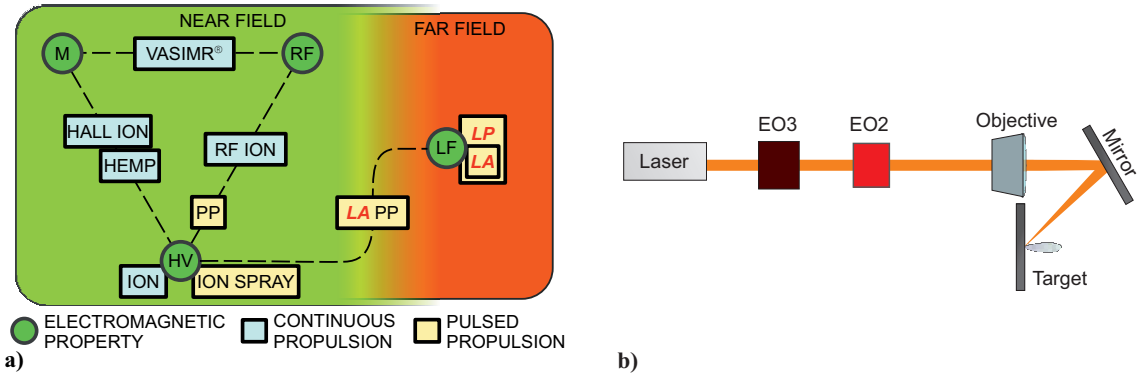

Figure 1. a) Exemplary categories of electric propulsion from the viewpoint of electrodynamics. Two essential categories, far and near field electrodynamics as well as pulsed and continuous propulsion, can be identified. b) Concept of the laser-ablative thruster comprising a pulsed microchip laser, an electro-optical device (EO2) for 2D lateral beam-steering, an electro-optical lens (EO3) with variable focus length, an f-theta object lens with fixed focal length, a plane mirror, and a metallic target.

spots has to be optimized for minimum surface degradation which means that each layer should exhibit a smooth surface.

Possible laser candidates for this concept are solid-state lasers with pulse energies in the μJ range with repetition rates that can be varied over several orders of magnitude. Compatibility with the corresponding space mission presumably does not allow the usage of high voltages, and, of course, the selected laser has to be qualified for operation in space which is the case for numerous types of solid-state lasers.

III. Research Strategy

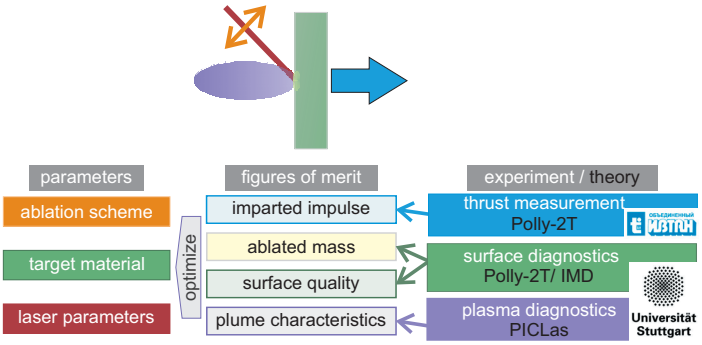

Figure 2. Research strategy for the development of the laser-ablative microthruster.

For research on this propulsion concept and the subsequent development of a laboratory prototype, the following issues are of importance, cf. Fig. 2: Beyond the basic figures of merit, imparted impulse, propellant consumption, and specific impulse, the surface quality of the target during its usage as a laser-ablative propellant has to be analyzed carefully. Additionally, as for any propulsion device, the divergence of the plume is important as well. With this concept, contamination of the bending mirror has to be avoided which is addressed here by oblique incidence of the laser beam.

The main parameters that influence the performance of the future thruster based on laser-matter interaction are related to the laser (pulse length τ, wavelength λ, fluence Φ_T, incidence angle ϑ, and polarization), the selection of the target material, and, with respect to interaction, the choice of a suitable ablation pattern that ensures sustainably precise thrust generation. Experimental work covers thrust measurements with a torsional balance, plasma diagnostics with Faraday cups and analysis of the target surface by profilometry. For the wide range and the multitude of operational parameters, these investigations are accompanied by hydrodynamic (HD) simulations on laser ablation. Supplementary Molecular Dynamics (MD) as well as

PIC-DSMC simulations are validated for this purpose as well.

A. Experimental Facilities

According to the research strategy summarized in Fig. 2 experimental facilities for thrust measurement, surface diagnostics and ablation parameters optimization have been designed and implemented. They have been described in detail in Ref. 9 and are thus only briefly summarized.

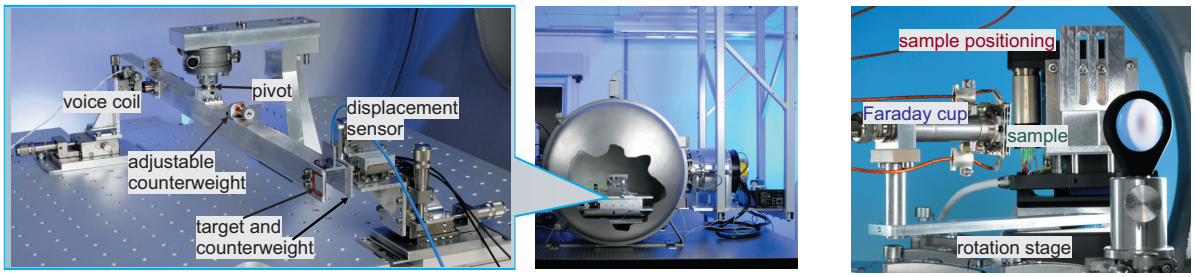

a) **b)**

Figure 3. a) left: torsional pendulum thrust balance; right: thrust balance vacuum chamber approx. 500 l (diameter 800 mm, length approx. 950 mm), b) Faraday cup plume diagnostics setup.

A torsional pendulum has been designed as a thrust balance for the development of a laser-ablative microthruster with the following criteria in mind: range of measurable thrust from sub-μN to approx. 1 mN, minimized influence of external vibrations, and a flexible, modular setup that leaves room for further modifications and improvements.

The balance setup inside its approx. 500 l vacuum chamber is shown in Fig. 3 a). The vacuum pumping system consists of backing pump and a 2650 l/s (N_2) magnetic bearing turbomolecular pump. To reduce vibration transmission from the pumping system the turbomolecular pump is mounted on the laboratory ceiling and attached to the chamber via a bellows connector. The balance arm and base have a breadboard design to allow for flexible positioning of components. They are installed on a vacuum compatible vibration isolation platform (Minus K). To further minimize the influence of external vibration the balance arm center of mass is kept on the rotational axis by using adjustable counterweights and copies of attached components. Flexural pivots are used as the torsional element and a range of pivots and interchangeable mounts is available. Voice coils (MotiCont) are used for calibration, active damping and as a force actuator for closed-loop operation. Additionally, a calibration method based on photon pressure using a thin-disk laser with up to 1 kW power has been demonstrated. Where necessary for alignment, suitable mechanical components have been included in the setup, e.g., adjustment screws for leveling of the balance mount and the base plate as well as translational stages for positioning of the capacitive displacement sensor and voice coils.

A commercial white light interferometer (Veeco NT9100) is used for analysis of the target before and after ablation. It provides information on single and multiple shot crater geometry, topography, and location. These measurements are used to determine surface roughness, estimate ablated material volume, and for checking crater size and locations for positioning and adjustment purposes.

Analysis of the plasma plume that results from each ablation event is of interest for gaining a better understanding of the laser ablation process, assessing the influence of changing surface roughness, and for the evaluation of problems with contamination. Information on charged plume components can be obtained from Faraday cup measurements. An overview of the setup inside an approx. 35 l vacuum chamber is given in Fig. 3 b). Positively charged plume components are collected with a negatively biased 5 mm ø aperture Faraday cup and the amplified signal is read out on an oscilloscope. The target is mounted on a 2-axis motorized translation stage setup which is used to shift a fresh propellant area for each ablation event. For measurements at different angular positions the Faraday cup is mounted on a motorized rotational stage with its rotational axis centered at the focus point on the sample. Measurements are usually done at $< 5 \cdot 10^{-6}$ mbar, which can be achieved after short pump down times with a 1550 l/s (N_2) turbomolecular pump vacuum system.

Two microchip lasers with 1064 nm wavelength and pulse energies of max. 80 μJ at 500 ps pulse length (Teem Photonics, Powerchip) and 1 mJ at 1 ns (Alphalas, Pulselas) are available for ablation experiments. Additionally to pulse length and energy, parameter variations include different target materials, spot sizes,

polarization, and different ablation patterns. The ablation pattern is currently controlled by either moving the target (ablation diagnostics) or a mechanical galvanometer scanner system that is set up outside the chamber (thrust measurements). A suitable EO beam-steering module is required to fully take advantage of the laser-ablative thruster concept, i.e., to avoid moving parts. Eligibility criteria for beam steering modules are deflection angle range and accuracy, scanning speed, laser damage threshold, beam distortions introduced by the scanner, low losses at the laser wavelength, and suitability as a satellite component, e.g., power consumption/required voltages and compatibility with space environment. Electro-optial beam steering is based on changes of the refractive index resulting from an applied electric field. One possible commercially available technology, KTN ($KTa_{1-x}Nb_xO_3$) crystal based steering modules from NTT-AT,[10] has been evaluated. This scanning technology is Kerr effect based and exhibits a large scanning angle due to the fact that the electric field is the sum of the applied external field and the field from a space charge distribution that results from electrons injected into the crystal from the electrode.[10,11]

Whereas the crystals and coatings have sufficient damage thresholds (up to 2.8 J/cm^2 at 10 ns, s-on-1, measured at DLR's testing facilities for laser-induced damage) and large scanning angles of approximately $\pm$ 100 mrad at less than $\pm$ 300 V have been demonstrated,[10] the technology also has some drawbacks: The refractive index modulation also results in a cylindrical lens,[10] the scanners require good temperature stabilization[12] and whereas it is inferred that the space charge distribution facilitates the large scanning angle,[10,11] the distribution of trapped charges is also influenced by applied voltage and the individual composition crystal.[13]

These effects would have to be sufficiently compensated by additional components. Vibrations of the KTN crystals due to electrostriction[14] also have to be taken into account in thruster noise considerations when high voltages are applied for large scanning angles. As an alternative to KTN crystals, beam steering might also be achievable by using liquid crystal technologies. Methods for three-dimensional beam shaping[15] and fast beam deflection[16,17] are known and demonstrated. Nevertheless, limitations in the applied voltages, ambient temperature, and pressure will add more complexity to the approach. Acousto-optical deflectors as another alternative would lead to high power consumptions due to the HF requirements solely for the purpose of beam steering, which would reduce the engine efficiency dramatically. In any case the damage thresholds of the optical components further reduce the variety of possible solutions. As a tradeoff choice with current technologies microelectro-mechanical systems (MEMS) might offer beam steering capabilities while introducing only minor inertia forces to the global system. Especially resonant MEMS scanning devices and deformable mirror devices offer high speed beam control suiting the task of a wide thrust-range laser-ablative thruster concept.

B. Hydrodynamic Simulations with Polly-2T

The theoretical description of laser-matter interaction with metals follows the so-called Two-Temperature-Model[18] (TTM) considering the target material to consist of two subsystems, namely the electron gas with temperature T_e where the laser energy is absorbed

$$c_e\left(T_e\right)\frac{\partial T_e}{\partial t} = \nabla\left[\kappa_e\left(T_e\right)\nabla T_e\right] - \gamma_{ei}\left(T_e - T_i\right) + S\left(\vec{r},t\right) \tag{1}$$

and the ion lattice with temperature T_i receiving the absorbed energy from the electron gas by electron-phonon coupling

$$c_i\frac{\partial T_i}{\partial t} = \gamma_{ei}\left(T_e - T_i\right) \tag{2}$$

with the specific heat c_j $(j = e, i)$ of the two subsystems, the electron heat conductivity κ_e, the electron-phonon coupling coefficient γ_{ei}, and the laser pulse energy density S. Electron-phonon coupling is related to a material-specific coupling time[19] $\tau_i = c_i/\gamma_{ei}$ that is needed for material heating, whereas $\tau_e = c_e/\gamma_{ei}$ is the characteristic time for electron cooling. For the propellant materials used in this study, literature data on τ_e are found to be in the femtosecond range (aluminum: 126 fs,[20] and 67 fs,[21] resp.; gold: 184 fs,[20] and 571 fs,[21] resp.). Electron-phonon coupling times τ_i of both materials are reported to be in the picosecond range and differ by one magnitude (aluminum: 4.3 ps,[22] 6.21 ps,[20] and 4.27 ps,[21] resp.; gold: 119 ps,[22] 66.4 ps,[20] and 70.6 ps,[21] resp.). The data based on Ref. 20 were derived using the Fermi velocity of the electrons as given in Ref. 23.

According to Ref. 19, the three time scales τ_e, τ_i, and the laser pulse length τ_L are crucial for the characteristics of the laser ablation process with metals. Whereas various reasonable simplifications of Eqs. 1 and 2 exist for these different laser-matter interaction regimes,[19] we performed 1D hydrodynamic simulations based on the full set of TTM equations for a great range of laser pulse lengths. For this purpose, we used the Lagrangian code Polly-2T from the Joint Institute of High Temperatures (JIHT) at the Russian Academy of Sciences (RAS), Moscow, which is described in great detail in Ref. 24. With some limitations, this simulation code is accessible by a web interface as an open-access tool as well[25,a].

IV. Operational Parameters

Laser ablation is a complex physical process which is influenced by a broad range of parameters. The mass of the ablated material $m = \int \mu_a dA_s$, its velocity $\langle v_{jet} \rangle = g \cdot I_{sp}$ and the impulse coupling coefficient $c_m = m \cdot \langle v_{jet} \rangle / E_L = \langle F \rangle / \langle P_L \rangle$ defined as the ratio of the imparted impulse to the employed laser pulse energy (or mean thrust to average optical power) depend on the selection of propellant material and laser. In general, relevant laser parameters are pulse length τ_L and wavelength λ. Moreover, for a specific thruster layout, the resulting fluence Φ_T in the spot of focused laser beam and even the beam incidence angle ϑ and its polarization have to be taken into account. Therefore, parameter studies by simulations and experiments are carried out in order to find an optimum working point for the laser-ablative microthruster.

A. Ablated Mass

For ultrashort-pulse laser ablation, results from hydrodynamic simulations comprise the ablation depth in the point of time where the ablation process is finished and the target surface has solidified again. With longer laser pulses, however, in the case of rather long lasting material vaporization, the asymptotic limit is derived from the temporal course of mass loss. The dependency of the ablation depth d_a from the fluence at the target surface Φ_T is given by

$$d_a = \frac{1}{\alpha} \ln \xi \tag{3}$$

with the optical absorption coefficient α, the normalized fluence $\xi = \Phi_T / \Phi_0$ comprising Φ_0 as the threshold fluence for laser ablation.[26] Simulation results are found to be in good agreement with Eq. 3, as can be seen from the corresponding fit functions in Fig. 4 a). The fit results for Φ_0 and α can be found in Table 1 (see p. 9). Comparison with experimental data from Ref. 27 and 28 shows rather good agreement for Φ_0 with aluminum (though at $\vartheta = 15°$, p-polarized in Ref. 28). The absorption coefficient α is significantly lower than literature data for α at room temperature.[26] This can be deduced to the strong dependence[24] of α from T_i, T_e and ϱ since large temperature and pressure gradients occur during the laser ablation event.

Keeping Eq. 3 in mind, one should expect that a Gaussian fluence distribution on the target surface would yield an ablation profile close to a Gaussian shape. However, profilometric analysis of craters on aluminum induced by a 500 ps laser pulse reveals a significant difference which is depicted in Fig. 4 b): Whereas the central part of the crater exhibits fair accordance with a Gaussian, cf. the corresponding datafits, an outer crater rim with positive surface elevation is found which can be ascribed to lateral motion of the molten material[26] and/or material re-deposition.[29] Though the aspect ratio of crater elevation to diameter is rather low, these irregularities might lead to a rather rough target surface in the long run, in conjunction with reduced precision of the amount and direction of the imparted impulse.

Therefore, attention has to be paid on the right selection of suitable laser parameters yielding a smooth target surface after ablation layer by layer. Based on the findings in Ref. 22, the current experimental strategy focuses on laser ablation in the so-called picosecond regime where $\tau_L << \tau_i$. In this case, the heat affected zone (HAZ) in the target beyond the ablated material is rather small ($d_{\mathrm{HAZ}} \approx 200\ nm << d_s$). Hydrodynamic simulations show that material spallation of liquid layers induced by strong tensile waves following the initial shock are a main ablation mechanism here, whereas material vaporization, which is dominant in the nanosecond regime ($\tau_i << \tau_L$), plays a minor role.

[a]Povarnitsyn, M. E., "Virtual Laser Laboratory," Joint Institute of High Temperatures (JIHT) at the Russian Academy of Sciences (RAS), Moscow, URL: http://vll.ihed.ras.ru/

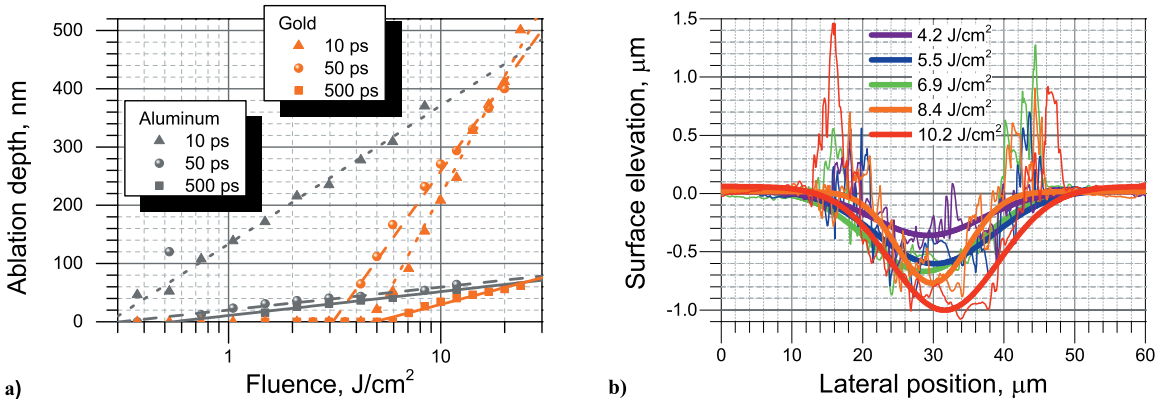

Figure 4. a) Ablation depth as a function of laser pulse fluence at the target surface for aluminum and gold, various pulse lengths, results from hydrodynamic simulations. Laser parameters: $\lambda = 1064$ nm, circular polarization, incidence angle $\vartheta = 0°$, b) Cross-section of ablation craters on aluminum (thin curves) and corresponding Gaussian datafits (thick curves). Laser parameters: $\lambda = 1064$ nm, $\tau_L = 500$ ps, p-polarization, incidence angle $\vartheta = 15°$.

B. Specific Impulse

Using an analytical model, Sinko and Phipps[2] report

$$I_{sp}\left(\Phi_T\right) = \sqrt{\frac{2 \cdot \Phi_0 \left(T\xi - 1\right)}{g^2 \left(\varrho/\alpha\right) \ln \xi}} \tag{4}$$

for low fluences in the so-called vaporization regime, together with a smooth transition, depending on the degree of ionization, to the high fluences of plasma regime with

$$I_{sp}\left(\Phi_T\right) = 442 \frac{A^{1/8}}{\Psi^{9/16}} \left(\Phi_T \lambda / \sqrt{\tau_L}\right)^{1/4} \tag{5}$$

with ϱ being the density of the ablated material, T the transmissivity to the ablation region, A the mean atomic mass, and $\Psi = A/2\left[Z^2\left(Z+1\right)\right]^{1/3}$ a mass-weighted ionization factor containing the degree of ionization Z. However, the validity of Eq. 5 is not given for ultra-short laser pulses. Hence, for the analysis of simulation results, our computational results were fitted with a simple exponential function $I_{sp}\left(\Phi_T\right) = \sum_{j=1}^{2} a_j \left[1 - \exp\left(-\left(\Phi_T - b_j\right)/c_j\right)\right]$ where a_j, b_j, c_j are datafit parameters.

As it can be seen from Fig. 5 a) and Table 1, the specific impulse strongly depends on both material and pulse length. The most significant issue is the sudden increase of $I_{sp,max} = a_1 + a_2$ with increasing pulse length. This phenomenon marks the transition from the ultrashort-pulse to the nanosecond-pulse regime occurring at $\tau_L >> \tau_i$ which is the case at $\tau_L = 50\ ps$ for aluminum, and $\tau_L = 500\ ps$ for gold, resp. Though long pulses yield a rather high specific impulse, the surface inside the ablation craters is reported to be rather rough in contrast to the ultrashort-pulse regime.[19] Roughness inside the crater in conjunction with large crater rims might lead to high surface roughness of the propellant in long term operation.

Experimental data from temporally and spatially resolved plume analysis with Faraday cups[30] of laser ablation at $\tau_L = 500$ ps even show higher values for the specific impulse, cf. Table 1. It should be noted, however, that only charged particles can be detected with Faraday cups but not neutral ones. Therefore, as already reported in Ref. 8, discrepancies of more than one magnitude between the velocity of the jet and the speed of its charged components may occur.

C. Thrust-to-Power Ratio

In electric propulsion, the thrust-to-power ratio $c_{t/p}$ is a common figure of merit

$$c_{t/p} = F/P_{el} \tag{6}$$

where P_{el} denotes the electrical power required to obtain the thrust F. In laser propulsion technology, this definition is split up into

$$c_{t/p} = \eta_{eo} \cdot c_m \tag{7}$$

with the electro-optical energy conversion efficiency η_{eo} of the employed laser system and the impulse coupling coefficient c_m which depends both on optical and material parameters. Hence, in contrast to Eq. 6, Eq. 7 allows to distinguish between technological efficiency and specific process characteristics of this propulsion technology. Typical values for η_{eo} are in the range of 10 % whereas generally, in the nanosecond-pulse regime, the thrust-to-power ratio c_m for the specific process of laser ablation amounts up to 30 μN/W for metals, and up to 300 μN/W for polymers, taking aluminum, and polyoxymethylene, resp., as two representative target materials.[31] According to Ref. 2, the maximum of the impulse coupling coefficient is found at $\xi_{\text{opt}} \approx 4.2$.

As an example, various results from HD simulations as well as experimental data on impulse coupling from measurements at the torsional balance are shown in Fig. 7 a) (see p. 11).

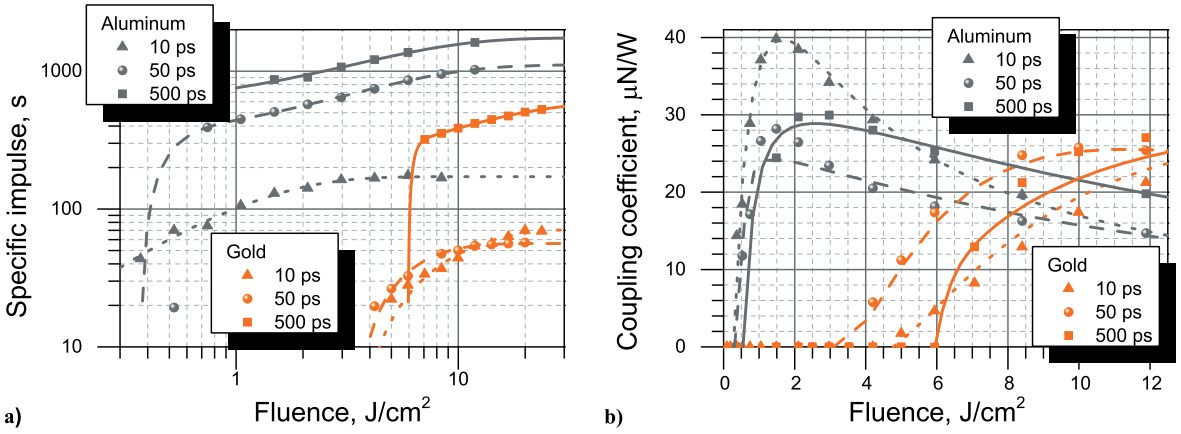

Figure 5. a) Specific impulse I_{sp} and b) Momentum coupling coefficient c_m vs. fluence Φ_T for aluminum and gold for various pulse lengths τ_L at circular polarization, incidence angle $\vartheta = 0°$. Results from hydrodynamic simulations.

Since a rather good correlation between experimental and theoretical data is found, extended parameter studies were carried out by HD simulations for the assessment of an optimum working point of the thruster, cf. Fig. 5 b). Some results for relevant laboratory laser setups are shown in Table 1.

Table 1. Figures of merit for laser-ablative micropropulsion with aluminum and gold, resp., as propellant for various pulse lengths τ_L with $\lambda = 1064$ nm, $\vartheta = 0°$, results from hydrodynamic simulations: Ablation threshold Φ_0, optical absorption coefficient α, specific impulse I_{sp}, fluence Φ_{opt} for optimum momentum coupling, and optimum coupling coefficient c_m. ξ_{opt}: see text. Additionally, own experimental data [in squared brackets] for aluminum, $\tau_L = 500$ ps, $\vartheta = 15°$, p-polarization are given as well as literature data (in brackets).

	τ_L	Φ_0	α	$I_{\text{sp,max}}$	Φ_{opt}	ξ_{opt}	$c_m\,(\Phi_{\text{opt}})$
Target	ps	J/cm^2	10^4 cm^{-1}	s	J/cm^2	-	μN/W
Al	10	0.27 ± 0.02 (0.37)[27]	9.7 ± 0.3 (100)[26]	172 ± 3	1.6	5.9 (4.2)[2]	39.7
Al	50	0.31 ± 0.04	58 ± 3 (100)[26]	1110 ± 15	1.5	4.8 (4.2)[2]	28.2
Al	500	0.55 ± 0.06 [1.6 ± 0.5][28]	56 ± 3 (100)[26]	1741 ± 70 [4700 ± 30][30]	2.6	4.7 (4.2)[2]	28.9
Au	10	4.8 ± 0.1	3.4 ± 0.1 (77)[26]	72 ± 5	18.9	3.9 (4.2)[2]	26.7
Au	50	3.1 ± 0.1	4.5 ± 0.2 (77)[26]	56 ± 1	11.3	3.6 (4.2)[2]	25.5
Au	500	4.9 ± 0.4	24 ± 2 (77)[26]	594 ± 8	20.3	4.1 (4.2)[2]	28.0

Lasers differ with respect to the wavelength of the emitted light, depending on the chosen laser medium. Solid-state lasers typically emit near-infrared (NIR) radiation where prominent wavelengths are 1064 nm

(Nd:YAG laser), 1030 nm (Yb:YAG laser), and 800 nm (Titanium:Sapphire laser), resp. Figure 6 shows the impact of the laser choice on momentum coupling. For moderate fluences below Φ_{opt}, the slight deviations in momentum coupling can easily be explained by the differences in $R(\lambda)$ which is the target reflectivity at room temperature yielding greater momentum with higher light absorption. Nevertheless, with fluences beyond Φ_{opt} very high temperatures and plasma formation occurs in the heat affected layer. Hence, the permittivity of the material strongly changes during the laser pulse which turns the picture. The complex underlying physical phenomena are described in detail in Ref. 24.

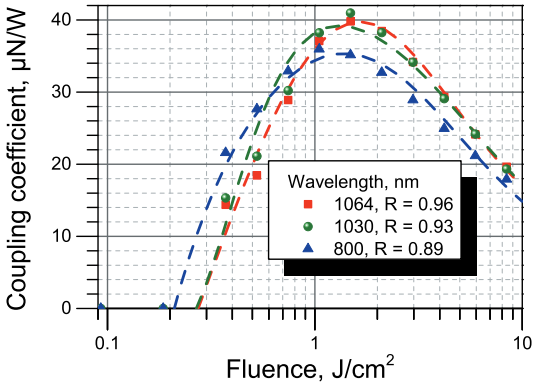

Figure 6. Momentum coupling coefficient c_m vs. fluence Φ_T at $\tau_L = 10\ ps$, circular polarization, incidence angle $\vartheta = 0°$ for various laser wavelengths λ.

As a possible source of thrust noise, it should be considered that during scanning a rather extended area in an ablation pattern, the incidence angle at the surface might vary by $\Delta\vartheta = \pm 1°$. Though the changes in the fluence on the target surface can easily be compensated by modifications of the laser pulse energy, the specific dependency of the permittivity on the incidence angle might yield changes in momentum coupling by 1 % and beyond as derived from hydrodynamic simulations for aluminum at $\tau_L = 10\ ps$ with $\vartheta = 30 \pm 1°$, circular polarization. This phenomenon can be ascribed to the rather sharp threshold criterion for spallation with ultrashort laser pulses at a maximum tensile strength of approximately 2 GPa, as chosen for numerical simulations. Therefore, the system is rather sensitive to slight parameter changes concerning the question whether an additional target layer is ablated or not. In any case, experimental work could shed some light into this problem and answer the question whether this is rather a numerical artifact or should be seriously taken into account for choosing a stable operating fluence being insensitive to slight parameter variations which was observed as well for certain fluences.

V. Thrust Generation in the Micronewton Range

In Ref. 2, Phipps et al. report on two types of laser-ablative microthrusters (so-called laser plasma thrusters, LPT) which are classified according to the employed laser pulse length as millisecond LPT, and nanosecond LPT, resp. Similar to our concept, the latter one operates with ablation of metals yielding high I_{sp} and low c_m, however, with moving components. On the other hand, high thrust at low I_{sp} is featured by the ms-LPT which uses, among others, energetic polymer targets as propellant material.

In our case, we follow this idea of thruster classification based on τ_L, since we have found two basically different regimes of laser ablation. Envisioning a laboratory prototype of this thruster, we introduce the term MICROLAS for our concept. Based on the aforementioned parameter studies, its preliminary figures of merit can be derived as shown in Table 2.

For the figures of merit in Table 2, $d_s = 40\ \mu$m, $\eta_{eo} = 0.1$, $\langle F \rangle = 10\ \mu$N were anticipated and $\Phi = \Phi_{\text{opt}}$ was selected for MICROLAS. It can be seen that the ns-MICROLAS concept outperforms the ps-thruster with respect to the specific impulse. However, it is likely that in the ns-case the increasing surface roughness might infer the thruster precision. This could be overcome with the ps-concept, but at the expense of increasing propellant consumption.

The thrust-to-power ratio for the MICROLAS concept amounts around 3 μN/W and is nearly independent from propellant choice and laser pulse length. It should be noted, however, that oblique incidence of

Table 2. Figures of merit for different layouts of the laser-ablative microthruster MICROLAS in comparison with ns-LPT[8] with aluminum and gold, resp., as propellant: pulse length τ_L, pulse energy E_L, operating fluence Φ, minimum impulse bit Δp, specific impulse I_{sp}, thrust-to-power ratio $c_{t/p}$, propellant consumption ΔM.

		τ_L,	E_L	Φ	Δp	I_{sp}	$c_{t/p}$	ΔM
Target	Concept	ps,	μJ	J/cm^2	nNs	s	μN/W	g/y
Al	ps-MICROLAS	10	20.1	1.6	0.80	131	4.0	245
Al	ns-MICROLAS	500	32.7	2.6	0.94	1017	2.9	31.6
Al	ns-LPT	4000	13.2	34.6	1.47	1120	11.1	29.0
Au	ps-MICROLAS	10	238	18.9	6.34	66	2.7	493
Au	ns-MICROLAS	500	255	20.3	7.14	506	2.8	62.2
Au	ns-LPT	4000	13.2	63.6	0.90	3660	6.8	8.8

the laser beam is necessary in order to avoid optics contamination. Assuming an incidence angle of $\vartheta = 45°$ the twofold laser power might be required to achieve the same thrust, not only to keep a constant fluence under oblique incidence but also to take into account for reflectivity changes of the target surface due to incidence angle and polarization.

First thrust measurements show low thrust noise behavior close to the requirements of 0.1 μN/$\sqrt{\text{Hz}}$ in the (e)LISA mission (Fig. 7 b), dashed line).

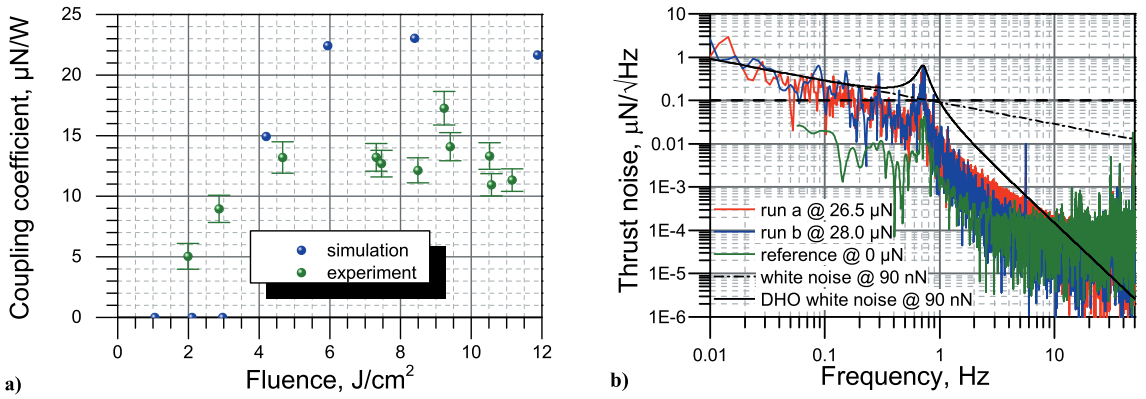

Figure 7. a) Experimental data and simulation results for the coupling coefficient in laser-ablative propulsion. Propellant target: aluminum; b) Spectral thrust noise in the range from 10 mHz to 50 Hz for 26.5 μN and 28 μN thrust. A one minute thrust free measurement serves as a reference. Thrust measurements have been corrected for linear drift and thrust offset. Furthermore a cos^6 window was applied before the FFT. λ = 1064 nm, $d_s \approx$ 270 μm, $\langle P_L \rangle$ = 2.27 $\pm$ 0.01 W, τ_L = 8 ns, f_{rep} = 1 kHz, thrust time t = 350 s. Noise requirement of LISA mission (horizontal dashed line), the noise signature of an ideal white noise measurement (dot dashed line) as well as the expected result for white noise measured with the torsion balance (solid line) are indicated.

The results can be interpreted with respect to the driven harmonic oscillator (DHO) behavior of the torsion balance. A white noise source with an amplitude of 90 nN is indicated by the dot dashed line in Fig. 7 b). The same source driving a DHO with a resonance at 0.72 Hz and a damping constant of 0.37 s^{-1} would lead to the solid line. The differences of both lines indicate the shift needed to compensate measurement artifacts in the noise spectrum. Therefore, the noise around 0.72 Hz is overestimated, whereas the noise above 1 Hz is underestimated. The difference between the dot dashed and the solid line at 15 Hz is great enough that obviously the restriction to 0.1 μN/$\sqrt{\text{Hz}}$ is not fulfilled any longer. Nevertheless, other noise sources in the measurement system cannot be excluded as indicated by the reference measurement (green).

VI. Conclusion and Outlook

In an experimental and theoretical parameter study we have outlined our concept of the laser-ablative microthruster MICROLAS. The absence of moving components promises highly precise operation with very small impulse bits. With respect to the laser-induced jet generation, we identified two different regimes, namely nanosecond and picosecond regime, depending on the laser pulse length with regard to material specific properties.

Whereas high ablation precision and therefore precise thrust generation is more likely in the picosecond regime, the specific impulse might be disadvantageous high in comparison with the nanosecond regime. However, in any case, suitable patterns for the laser ablation scan over the propellant surface have to be found and evaluated with both profilometric surface analysis and corresponding thrust measurements. Moreover, the divergence of the ablation jet and possible droplet formation have to be carefully analyzed for both regimes in order to assess the suitability of various laser parameter sets. Up to now, simulations are limited here mainly to the 1D case though promising developments in Molecular Dynamics and PIC-DSMC are in progress.

The long term stability of laser-ablative microthrusters based on the reported concept will depend on the continuous functionality of all participating components. Starting with the electric circuit controlling the laser and beam steering units, continuing with the latter. The laser beam must reach the propellant undisturbed. The surface of the propellant material itself again must not degrade unboundedly in order to sustain operationality. The result of the first thrust measurements are quite promising and close to actual mission requirements. Therefore, future aspects of our implementations of the concept will not only focus on avoiding degenerating effects, but also to introduce servo loops as it would be the case for a real satellite mission. With this approach we are searching to clearly identify the qualities and obstacles for a long term operation of our thruster concept.

Acknowledgments

We greatfully appreciate Dr. M. E. Povarnitsyn's sound contribution in inspiring scientific discussions and especially by providing us with the Polly-2T simulation code. The contributions of our former master students Vitalij Fedotov, Torben Sehnert, and Christian Illg considering torsion balance setup and plume diagnostics is thankfully acknowledged as well.

References

[1]Leach, R., and Neal, K. L. "Discussion of Micro-Newton Thruster Requirements for a Drag-Free Control System," *16th Annual AIAA/USU Conference on Small Satellites*, SSC paper 02-VIII-1, 2002.

[2]Phipps, C., et al. "Review: Laser-Ablation Propulsion," *J. Propul. Power*, Vol. 26, No. 4, 2010, pp. 609-637.

[3]Sutton, G. P., and Biblarz, O., *Rocket Propulsion Elements*, 7th ed., John Wiley & Sons, New York, 2001, Chap. 19.

[4]Keller, A., et al., "Feasibility of a Down-Scaled HEMP-Thruster," *32nd International Electric Propulsion Conference*, IEPC paper 138, 2011.

[5]Longmier, B. W., et al., "Performance Measurements and Technology Demonstration of the VASIMR® VX-200,"' *In AGU Fall Meeting Abstracts*, Vol. 1, 2010, pp. 1890

[6]Tsay, M., Hohman, K., and Olson, L., "Micro RF Ion Engine for Small Satellite Applications,"' *23rd Annual AIAA/USU Conference on Small Satellites*, SSC paper 09-II-1, 2009.

[7]Molina-Cabrera P., et al., "Pulsed Plasma Thrusters: a Worldwide Review and Long Yearned Classification," *32nd International Electric Propulsion Conference*, IEPC paper 340, 2011.

[8]Phipps, C. R., Luke, J. R., and Helgeson W. D., "3ks Specific Impulse with a ns-Pulse Laser Microthruster," *29th International Electric Propulsion Conference*, IEPC paper 319, 2005.

[9]Karg, S., Fedotov, V., Sehnert, T., and Eckel, H.-A., "Laser Propulsion Research Facilities at DLR Stuttgart," *High Power Laser Ablation / Beamed-Energy Propulsion 2014* [CD-ROM].

[10]Yagi, S., and Fujiura K., "Electro-Optic KTN Devices ," *8th International Conference on Laser Assisted Net Shape Engineering*, Physics Procedia, Vol. 56, 2014, pp. 40-47.

[11]Nakamura K., Miyazu, J., and Sasaura, M., "Wide-Angle, Low-Voltage Electro-Optic Beam Deflection

Based on Space-Charge Controlled Mode of Electrical Conduction in $KTa_{1-x}Nb_xO_3$", *Appl. Phys. Lett.*, Vol. 89, 2006, pp. 131115.

[12]Huang C., et al., "Trapped Charge Density Analysis of KTN Crystal by Beam Path Measurement", *Opt. Express*, Vol. 22, No. 7, 2014, pp. 7783-7789.

[13]Imai, T., Miyazu, J., and Kobayashi, J., "Charge Distributions in $KTa_{1-x}Nb_xO_3$ Optical Beam Deflectors Formed by Voltage Application ," *Opt. Express*, Vol. 22, No. 12, 2014, pp. 14114-14126.

[14]Toyoda, S., Ueno, M., Yagi, S., and Kobayashi, J., "First Estimation of Power Consumption of $KTa_{1-x}Nb_xO_3$ Crystal upon Application of High Voltage under High Frequency", *Appl. Phys. Express*, Vol. 6, No. 12, 2013, pp. 122601.

[15]Nathan D., et al., "Use of a Microelectromechanical Mirror for Adaptive Optics in the Human Eye," *Opt. Lett.*, Vol. 27, No. 17, 2002, pp. 1537-1539.

[16]Date M., et al., "High Speed Optical Deflector with sub-Micron Droplet Polymer Dispersed Liquid Crystal", *Technical Digest, CLEO/PacificRim'95*, 1995.

[17]Miyajima, H., et al., "A MEMS Electromagnetic Optical Scanner for a Commercial Confocal Laser Scanning Microscope", *J. Microelectromech. Syst.* , Vol. 12, No. 3, 2003, pp. 243-251.

[18]Anisimov, S. I., Kapeliovich, B. L., and Perel'man, T. L., "Electron Emission from Metal Surfaces Exposed to Ultrashort Laser Pulses," *Sov. Phys.-JETP*, Vol. 39, No. 2, 1974, pp. 375-377, *Zh. Eksp. Teor. Fiz*, Vol. 66, Feb. 1974, pp. 776-781.

[19]Chichkov, B. N., Momma, C., Nolte, S., von Alvensleben, F., Tuennermann, A., "Femtosecond, Picosecond and Nanosecond Laser Ablation of Solids," *Appl. Phys. A*, Vol. 63, No. 2, 1996, pp. 109-115.

[20]Batani, D., "Laser Ablation and Laser Induced Plasmas for Nanomachining and Material Analysis," *Functionalized Nanoscale Materials, Devices and Systems*, edited by A. Vaseashta and I. N. Mihailescu, NATO Science for Peace and Security Series B: Physics and Biophysics, Springer Netherlands, 2008, pp. 145-168.

[21]Huettner, B., and Rohr, G., "On the Theory of ps and sub-ps Laser Pulse Interaction with Metals. II. Spatial temperature distribution," *Appl. Surf. Sci.*, Vol. 126, No. 1-2, 1998, pp. 129-135.

[22]Cheng, J., et al. "Effects of Laser Operating Parameters on Metals Micromachining with Ultrafast Lasers," *Appl. Surf. Sci.*, Vol. 256, No. 5, 2009, pp. 1514-1520.

[23]Kittel, C., *Introduction to Solid State Physics*, 5th ed., John Wiley & Sons. Inc., New, York, 1976, Chap. 6.

[24]Povarnitsyn, M. E., Andreev, N. E., Levashov, P. R., Khishchenko, K. V., and Rosmej, O. N., "Dynamics of Thin Metal Foils Irradiated by Moderate-Contrast High-Intensity Laser Beams," *Phys. Plasmas*, Vol. 19, No. 2, 2012, pp. 023110.

[25]Scharring, S., Foerster, D. J., Eckel, H.-A., Roth, J., and Povarnitsyn, M., "Open Access Tools for the Simulation of Ultrashort-Pulse Laser Ablation," *High Power Laser Ablation / Beamed-Energy Propulsion 2014* [CD-ROM].

[26]Baeuerle, D., *Laser Processing and Chemistry*, 3rd ed., Springer-Verlag, Berlin, 2000, Chaps. 10, 13.

[27]Cheng, J., et al. "Single-Pulse Drilling Study on Au, Al and Ti Alloy by Using a Picosecond Laser," *Appl. Phys. A*, Vol. 95, No. 3, 2009, pp. 739-746.

[28]Illg, C., "Plasma Characterization for Laser-Ablative Satellite Microthrusters," Diploma thesis, Institut fuer Strahlwerkzeuge, University of Stuttgart, Germany, 2013 (in German).

[29]Sinko, J. E., et al., "CO_2 Laser Ablation Area Scaling and Redeposition on Flat Polyoxymethylene Targets," *International Symposium on High Power Laser Ablation 2010*, edited by C. R. Phipps, AIP Conf. Proc., Vol. 1278, Melville, NY, 2010, pp. 538-547.

[30]Eckel, H.-A., Scharring, S., Karg, S., Illg, C., and Peter, J., "Overview of Laser Ablation Micropropulsion Research Activities at DLR Stuttgart," *High Power Laser Ablation / Beamed-Energy Propulsion 2014* [CD-ROM].

[31]Phipps, C. and Sinko, J. "Applying New Laser Interaction Models to the ORION Problem," *International Symposium on High Power Laser Ablation 2010*, edited by C. R. Phipps, AIP Conf. Proc., Vol. 1278, Melville, NY, 2010, pp. 492-501.